



## Letter

# Imaging of micro-steps on as-grown surface of sapphire with X-ray phase contrast technique

T.S. Argunova<sup>a,\*</sup>, V.G. Kohn<sup>b</sup>, J.-H. Lim<sup>c</sup>, V.M. Krymov<sup>a</sup>, A.V. Ankudinov<sup>a</sup>

<sup>a</sup> Ioffe Institute RAS, 194021 St. Petersburg, Russia

<sup>b</sup> National Research Centre "Kurchatov Institute", 123182, Moscow, Russia

<sup>c</sup> Pohang Accelerator Laboratory, 37673, Pohang, South Korea



## ARTICLE INFO

Communicated by S. Khonina

**Keywords:**

Synchrotron radiation  
Phase contrast  
Micro-steps  
Sapphire ribbons

## ABSTRACT

Basal-faceted sapphire ribbons grown using the Stepanov–LaBelle technology have a low density of surface steps. We present our results on a study of steps on the surface of a ribbon, misoriented relative to the singular face (0001) by several arc minutes. The ribbon has been characterized by means of in-line phase contrast imaging technique at Pohang Light Source, South Korea. It was shown for the first time that a step height of about 1  $\mu\text{m}$  can be determined directly from an image. The step height obtained using the phase contrast method was confirmed by atomic force microscopy measurements. We have found that the experimental contrast matches the theoretical simulations only if the calculated intensity profile has been convolved with a Gaussian function. The full width at half maximum of the Gaussian was independently got from previous measurements. We have obtained an analytical solution in the case of theoretical fully coherent phase contrast image. The inverse problem is easy to solve, since there is a direct proportionality between the contrast and the step height.

## 1. Introduction

Quantitative results of phase contrast X-ray imaging can only be obtained with a highly coherent synchrotron light source. Nowadays, the spatial coherence is provided by modern synchrotron radiation (SR) facilities [1–3], where the achievable transverse coherence length significantly depends on the size of the source [4]. The simplest X-ray imaging technique is the in-line phase-contrast imaging (PCI). The passage of an X-ray beam through an inhomogeneous object permits observing the internal structure of the object from the total phase shift along the beam paths. However, the variable phase shift cannot be recorded directly. The image is formed at a distance due to effects of focusing or defocusing, and quantitative information cannot be obtained without solving the inverse problem (see, e.g. [5–7]). Quantitative phase mapping implies recording intensity variations that should not vanish due to factors that reduce the transverse coherence length.

Some SR imaging experiments require a high photon flux. These include dynamic studies of changes in materials in real time; micro-imaging investigations with the spatial resolution beyond the micrometer limit [8,9], etc. Under such conditions, either high-intensity monochromatic radiation or a broad-band pink beam is demanded. The

high flux from a wiggler can cause a heat load on the monochromator and, as a consequence, distortion of its crystal lattice [10]. In the pink beam from a bending magnet, image details located away from the center of the pattern always vanish, and only the central part remains visible [11]. Under these conditions, there is no way of using phase-retrieval methods to solve the inverse problem. However, there always persists the method of computer simulations based on some simplified model of the object [12–14].

Accurate computer simulations of experimental intensities require knowledge of all parameters that can affect the theoretical profile, always calculated for fully coherent radiation by solving the Maxwell's equations. In this regard, the method for determining the transverse coherence length  $l_{tc}$  from the effective transverse size of the SR source  $w_s$  was proposed [4]. This method is based upon the visibility of Fresnel interference pattern that arise from an object with well-known parameters. In particular, an optical fiber was used, consisting of tungsten wire coated with amorphous boron.

In this paper, we assume that the damage of image contrast is due to the action of several factors that involve not only  $w_s$ . Non-smooth beryllium windows, aberrations caused by X-ray mirrors, Bragg diffraction from slightly curved crystal planes, vibrations, etc., can lead to a

\* Corresponding author.

E-mail addresses: [argunova@mail.ioffe.ru](mailto:argunova@mail.ioffe.ru) (T.S. Argunova), [kohnvict@yandex.ru](mailto:kohnvict@yandex.ru) (V.G. Kohn), [limjh@postech.ac.kr](mailto:limjh@postech.ac.kr) (J.-H. Lim), [V.Krymov@mail.ioffe.ru](mailto:V.Krymov@mail.ioffe.ru) (V.M. Krymov), [Alexander.Ankudinov@mail.ioffe.ru](mailto:Alexander.Ankudinov@mail.ioffe.ru) (A.V. Ankudinov).

<https://doi.org/10.1016/j.physleta.2024.129901>

Received 10 July 2024; Received in revised form 6 September 2024; Accepted 12 September 2024

Available online 13 September 2024

0375-9601/© 2024 Elsevier B.V. All rights reserved, including those for text and data mining, AI training, and similar technologies.

decrease in the transverse coherence of the beam. We obtain the real pattern from the ideal one by calculating convolution with a Gauss function for which the full width at half maximum (FWHM) is a free parameter. It is found that in many cases we can get the value of FWHM, which leads to excellent agreement between theory and experiment. It is shown for the first time that micrometer-high steps on as-grown surface of sapphire can be evaluated by using PCI technique. In doing so we determine the theoretical profile for fully coherent radiation by solving an analytical equation.

## 2. Experimental

The Pohang Light Source (PLS-II) in Pohang, South Korea, operates at an electron energy of 3.0 GeV. At the BL6C beamline a wiggler is inserted in the section of the storage ring. The alternating magnetic field of the periodic series of magnets has an induction of 2.0 Tesla applied in the vertical direction. The sinusoidal trajectory of the electron beam lies in the horizontal plane. The increase in intensity is due to large transverse oscillations of the electrons. Their angular deviations are wider than the natural opening angle  $\psi = mc^2/E_e \approx 35$  arc. sec., where  $m$  and  $E_e$  are the mass and energy of electrons,  $c$  is the speed of light. The smaller bending radius with respect to the bending magnets extends the spectral range towards higher energies: 23–50 keV.

In this range, the Si monochromator selects a peak at a given energy in a narrow spectral region  $\Delta E/E = 2.9 \times 10^{-4}$ , where  $E$  is the photon energy. In the BL6C optical hutch, the first crystal–monochromator was installed at a distance of  $r_s = 36$  m from the SR source. To cool the monochromator subjected to a thermal load of  $\sim 10$  kW liquid nitrogen was used. Residual heat could, however, cause bending of the crystal lattice planes.

To obtain X-ray images, monochromatic ( $\Delta E/E \approx 10^{-4}$ ) nearly parallel X-ray beam with energy of  $E = 23$  keV was used together with a pixelated detector. No other optical components were utilized. A sapphire ribbon was placed in the beam with its basal face perpendicular to the beam direction, and images were recorded at an intermediate object-detector distance,  $r_d$  (in the range from several to 20 cm). Apart from the source, sample, and detector, nothing else is required. The technique is distinguished for the simplicity of experimental scheme as repeatedly described previously (see, e.g. [15]).

To record X-ray images, a setup was utilized included a scintillator screen, magnifying lenses, and a low-noise charge-coupled device (CCD). The screen converted the X-ray image into the luminescent image projected by the lenses onto the CCD. Conversion screens were made from CsI, CdWO<sub>4</sub> and YAG:Ce scintillators virtually free of defects. The detector was equipped with a matrix PCO Edge (PCO AG, Kelheim, Germany). The matrix chip had a resolution of  $2560 \times 2160$  pixels and a size of  $6.5 \times 6.5 \mu\text{m}^2$ . We combined a scintillator and  $20\times$  objective lens with the CCD camera which led to an effective pixel size of  $0.325 \mu\text{m}$ . For each pixel, a 16 bit analogue digital conversion was performed. For each local measurement, electrical signal was stored to computer.

Fig. 1,a shows the experimental intensity distribution across the image of an optical fiber. The CCD is located at a distance of  $r_d = 10$  cm. The fiber consists of tungsten wire with a diameter of 15 microns coated with amorphous boron in such a way that the total fiber diameter is  $100 \mu\text{m}$ . The ideal fringe pattern simulated theoretically for the fully coherent beam from a point source is shown in Fig. 1,b. The calculations were performed by the XRWP (X-ray Wave Propagation) program [16]. We note that the minimum on the experimental curve in (a) is higher than on the theoretical one in (b), which indicates the influence of the parasitic noise. Without going into the details of this experiment, we can stress that the background must be removed for a correct comparison of the curves. Much more important, however, is that the intensity oscillations stand out strongly in (b) but disappear in (a).

We found that a good fit between simulated and experimental curves may often be obtained from the two-step calculations. First, an ideal fringe pattern is simulated using a point source. The real pattern is then

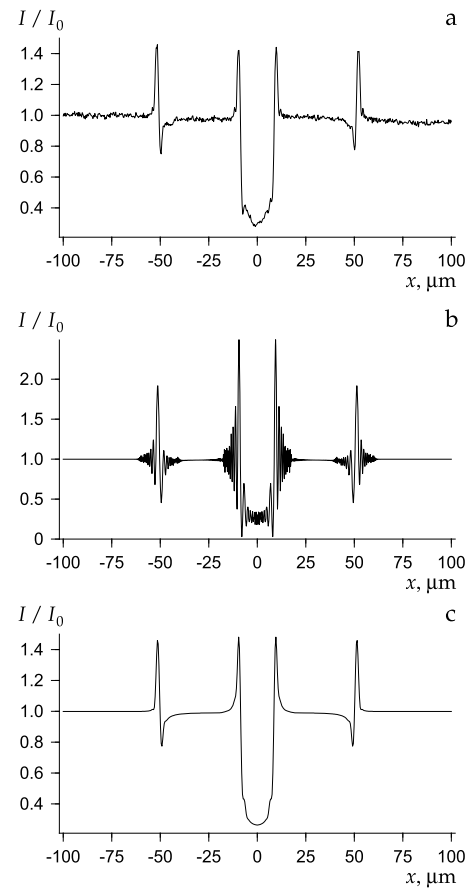


Fig. 1. Profiles of the relative intensity for the boron/tungsten fiber: (a) experimental,  $r_d = 10$  cm; (b) theoretical, calculated for fully coherent radiation; (c) calculated for smoothing of the features presented in the theoretical profile.

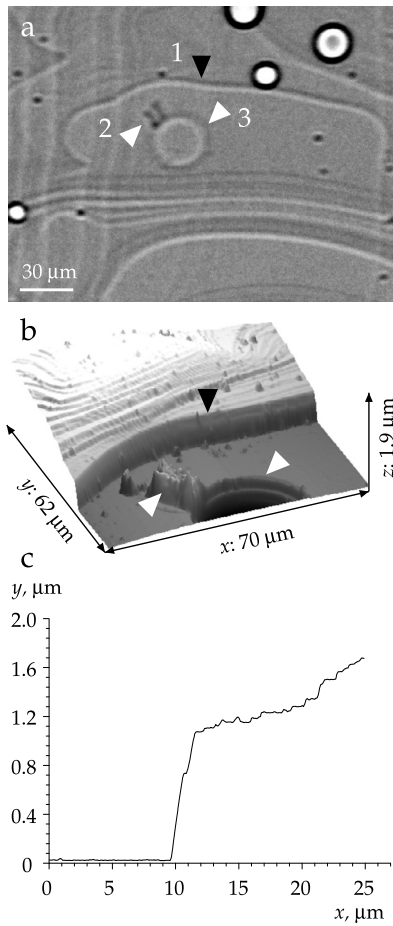
the convolution of the theoretical one and the Gaussian function. FWHM of the Gaussian is a parameter of the experimental setup as a whole. Once FWHM is established, it can be further used to determine the size of the observed image features.

Fig. 1,c illustrates the simulated curve obtained with a FWHM of  $1.8 \mu\text{m}$ . It is clear that simple convolution enables fitting the recorded data with fairly good accuracy. When the distance to the sample increased to  $r_d = 20$  cm, no noticeable changes occurred within the pattern, but the oscillation period became longer. Good agreement between simulation and experiment was obtained with a FWHM of  $2.0 \mu\text{m}$ . Furthermore, there was a very good match at a distance of 40 cm with a FWHM of  $3.6 \mu\text{m}$ .

We emphasize that the value of FWHM must depend on the distance  $r_d$ . If we assume that the FWHM is due to the size of the source alone, it should be two times larger when the distance is doubled. However, this dependence was not observed at any of the distances. The increase in FWHM was determined by two factors, and only one of them induced considerable changes with distance. We can conclude that averaging method is successful in setups where the factors that reduce coherence are unknown. Specifically, the convolution is useful in cases where the beam changes its position in space relative to the detector or vibrates with a period much shorter than the measurement time. In these cases, FWHM varied during the simulated optimization.

## 3. Results and discussion

Basal-faceted sapphire ribbons [17] have atomically flat (0001) faces and do not show surface steps under ideal conditions. However, the steps arise due to a slight thickness difference of the ribbon from the middle to the edges. In addition, when the surface deviates slightly from the



**Fig. 2.** (a) Phase contrast image of the area containing various defects in the sample. Black arrow points to step (1). White arrows point to particle (2) and pit (3). (b) 3D representation of AFM data. Arrows point to the same features as in (a). The AFM scan line is parallel to  $y$ -axis. The scan line intersects the step at the location indicated by the black arrow. One can see from Fig. 2,c that the step height changes slightly from 1 to 1.5  $\mu\text{m}$ . (c) Profile of the step height ( $y$ ,  $\mu\text{m}$ ) versus the distance across the step ( $x$ ,  $\mu\text{m}$ ) obtained from AFM data.

basal plane, it contains segments of flat faces interrupted by steps, and the density of steps is small. In this work we examined the basal-faceted ribbon grown from the melt by the Stepanov–LaBelle method with the growth rate  $1 \text{ mm} \times \text{min}^{-1}$ . Dimensions of the crystal were  $10 \times 0.4 \times 100$  ( $W \times H \times L$ )  $\text{mm}^3$ . The misorientation of the ribbon surface relative to the (0001) face was several minutes of arc.

In Fig. 2,a, light and dark long wavy lines can be seen. These are images of the steps on the ribbon surface. In addition, there are images of circular gas pores located in the bulk of the ribbon. Contrast of a gas pore image has a simple structure consisting of black ring along the edge and light color in the middle of the pore. We note that, unlike PCI, optical microscopy reveals only those pores that are located at or near the surface. The size of the pores  $\geq 2r_1$ , where  $r_1 = (\lambda r_d)^{1/2}$  is the radius of the first Fresnel zone for the distance  $r_d = 20 \text{ cm}$ . Here  $\lambda = hc/E = 0.054 \text{ nm}$  is the wave length,  $h$  is the Plank constant; then  $2r_1 = 6.57 \mu\text{m}$ . The transverse dimension of a pore can be measured directly from image pixels. The smallest pore on the right side of the phase image has a diameter of 46 pixels. For a given pixel size of  $0.325 \mu\text{m}$ , we obtain  $\approx 15 \mu\text{m}$ .

Interesting features of this picture are indicated by white arrows: a round area and its adjacent particle. One can distinguish black-and-white contrast of the round edge; and the sign of the contrast indicates that the area is a pit. Since the pit is near to the particle, it can be assumed that a hot metal piece hit the ribbon surface at a close distance

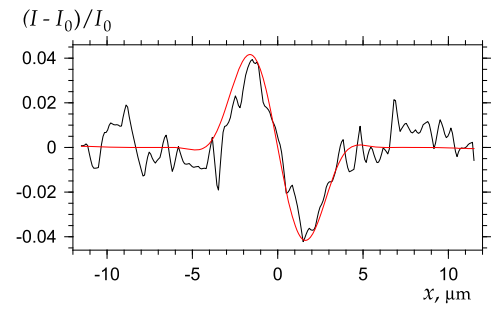


**Fig. 3.** Relative intensity profiles in a certain direction across the step: experimental (black) and calculated (red). The red profile is calculated by applying a Gaussian convolution to the ‘ideal’ intensity distribution obtained by the equation (1). The FWHM of the Gaussian is  $3 \mu\text{m}$ .

from the crystallization front. Then local overheating caused the formation of the pit.

Fig. 2,b represents the same region of the sample selected for surface morphology measurements. The micrometer-high surface topography was traced using atomic-force microscopy (AFM) technique. Measurements were performed with cantilevers in contact mode on the NT-MDT Integra-Aura installation. In 3D-AFM representation region of interest is within an area of  $70 \mu\text{m}$  ( $x$ )  $\times$   $62 \mu\text{m}$  ( $y$ )  $\times$   $1.9 \mu\text{m}$  ( $z$ ). The AFM scan line parallel to the  $y$ -axis intersects the step at the location indicated by the black arrow. One can see from Fig. 2,c that the step height changes slightly from 1 to 1.5  $\mu\text{m}$ .

In X-ray phase image (Fig. 2,a) the black arrow indicates the location where the phase contrast was measured. Unlike AFM profile, the phase contrast shows the height of the step due to the phase shift. Therefore, the contrast should be processed with caution. Images were recorded on a CCD and stored using TIFF format (16-bit) with a range of values from 0 to 65536. TIFF files were converted into a matrix. Then fragments were cut out from the matrix for processing the contrasts. In particular, an image fragment with dimensions of  $300 \times 300$  pixels was cut out from the region located between the morphological ‘slopes’ of the step line (Fig. 2,a). The distribution of the contrast was measured perpendicular to the step line.

The contrast profile associated with the black arrow in Fig. 2,a is shown by the black line in Fig. 3, where the minimum and maximum deviate from the average almost equally. Their behavior is completely consistent with the PCI theory for the image of vertical step. It can be shown that if the wave phase shift  $\phi$  introduced the step is less than unity:  $\phi \ll 1$ , then the relative intensity of the image (formed in parallel and monochromatic beam) is described by the function:

$$I/I_0 = 1 + \phi[S(x/x_0) - C(x/x_0)], \phi = K\delta t, x_0 = (\lambda r_d/2)^{1/2}. \quad (1)$$

Here  $S(x)$  and  $C(x)$  are the sine and cosine Fresnel integrals. The intensity profile calculated according to (1) has many fringes originating from the step region (data not shown). However, no oscillations are observed in the experimental intensity distribution (Fig. 3). The convolution with a Gaussian function results in smoothed profile shown by the red line in Fig. 3.

The contrast value determined from the plot is  $0.2\phi$ . Using the estimation of phase  $\phi = 0.2$ , obtained from the comparison of the experimental and simulated contrasts, and the decrement of the refractive index of sapphire  $\delta = 1.532 \times 10^{-6}$ , we find the step height  $t$  from the equation (1):  $t = 1.12 \mu\text{m}$ . It is concluded that the value of  $t$  agrees well with the AFM data.

#### 4. Summary

The main goal of this work is to demonstrate that PCI technique allows pretty accurate recording thickness changes ( $\sim 1 \mu\text{m}$ ) even at relatively large decrease in spatial coherence. The observable changes occur

within portion of the specimen area illuminated by the SR beam. For the first time, we have demonstrated that PCI gives the possibility to measure step heights on a micrometer scale directly from an image, which plays a valuable role in the study of as-grown crystal faces. Specifically, we investigated microsteps on a vicinal face of the sapphire ribbon slightly misoriented relative to the basal face. The height of the surface step was found to be  $\sim 1 \mu\text{m}$  and the finding was confirmed by atomic force microscopy measurements.

In this work, of particular interest is the comparison of experimental results with theoretical calculations. When the phase shift  $\phi$  introduced by a step is significantly less than unity, the intensity profile can be calculated as a power series of  $\phi$ , preserving the first contribution. The contrast is proportional to  $\phi$ , and therefore to the height of the step; it allows an analytical calculation using a simple formula.

Quantitative imaging requires a comparative analysis of calculated and experimental data. We provide an opportunity to account for the decrease in coherence by computing the convolution of the coherent contrast with Gaussian function. The FWHM of the Gaussian is determined in preliminary runs.

The PCI technique has advantages over probe microscopies and X-ray scattering methods, which include simplicity of the experimental setup and acceptable accuracy in estimating the micro-sizes. Image is recorded within available view field. On the other hand, the expansion of the area to be imaged can be obtained from moving the sample relative to the detector and assembling the view fields into a map.

#### CRediT authorship contribution statement

**T.S. Argunova:** Writing – review & editing, Investigation. **V.G. Kohn:** Writing – original draft, Software, Investigation, Conceptualization. **J.-H. Lim:** Investigation. **V.M. Krymov:** Investigation. **A.V. Ankudinov:** Investigation.

#### Declaration of competing interest

The authors declare that they have no known competing financial interests or personal relationships that could have appeared to influence the work reported in this paper.

#### Data availability

Data will be made available on request.

#### Acknowledgements

The work of T.S. Argunova was supported by the Ministry of Science and Higher Education of the Russian Federation; agreement No. 075-15-2021-1349. The work of V.G. Kohn was carried out within the state assignment of National research centre ‘Kurchatov Institute’. The work of V.M. Krymov and A.V. Ankudinov was carried out within the state assignment of Ioffe Institute.

#### References

- [1] A. Snigirev, I. Snigireva, V. Kohn, S. Kuznetsov, I. Schelokov, *Rev. Sci. Instrum.* **66** (1995) 5486.
- [2] P. Cloetens, R. Barrett, J. Baruchel, J.P. Guigay, M. Schlenker, *J. Phys. D, Appl. Phys.* **29** (1996) 133.
- [3] *ESRF HighLights*, 2022, p. 167.
- [4] V. Kohn, I. Snigireva, A. Snigirev, *Opt. Commun.* **198** (2001) 293.
- [5] P. Cloetens, W. Ludwig, J. Baruchel, D. Van Dyck, J. Van Landuyt, J.P. Guigay, M. Schlenker, *Appl. Phys. Lett.* **75** (1999) 2912.
- [6] D.M. Paganin, *Coherent X-Ray Optics*, Oxford University of Press, Oxford, 2006.
- [7] Ch. Zuo, J. Li, J. Sun, Y. Fan, J. Zhang, L. Lu, R. Zhang, W. Wang, L. Huang, Q. Chen, *Opt. Lasers Eng.* **135** (2020) 106187.
- [8] Y. Hwu, J.H. Je, G. Margaritondo, *Nucl. Instrum. Methods A* **551** (2005) 108.
- [9] A. Rack, F. Garcia-Moreno, C. Schmitt, O. Betz, A. Cecilia, A. Ershov, T. Rack, J. Banhart, S. Zabler, *J. X-Ray Sci. Technol.* **18** (2010) 429.
- [10] M. Ando, N. Sunaguchi, D. Shimao, A. Pan, T. Yuasa, K. Mori, Y. Suzuki, G. Jin, J.-K. Kim, J.-H. Lim, S.-J. Seo, S. Ichihara, N. Ohura, R. Gupta, *Phys. Med.* **32** (2016) 1801.
- [11] V.G. Kohn, T.S. Argunova, J.H. Je, *J. Phys. D, Appl. Phys.* **43** (2010) 442002.
- [12] S. Agliozzo, P. Cloetens, *J. Microsc.* **216** (2004) 62.
- [13] T.E. Gureyev, Y.I. Nesterets, A.W. Stevenson, P.R. Miller, A. Pogany, S.W. Wilkins, *Opt. Express* **16** (2008) 3223.
- [14] Ya.I. Nesterets, *Opt. Commun.* **281** (2008) 533.
- [15] T.S. Argunova, V.G. Kohn, J.-H. Lim, V.M. Krymov, S.Yu. Martyushov, *J. Surf. Investig.* **17** (Suppl. 1) (2023) S20.
- [16] V.G. Kohn, Available online: <https://xray-optics.ucoz.ru/XR/xrwp.htm>. (Accessed 5 September 2024).
- [17] N. Stoddard, M. Seitz, M. Seitz, W. Mushock, *J. Cryst. Growth* **530** (2020) 125306.